EUROPEAN ORGANIZATION FOR NUCLEAR RESEARCH (CERN)

CERN-LHCb-DP-2013-001
February 28, 2013

Performance of the Muon Identification at LHCb

The LHCb MuonID group [†]

Abstract

The performance of the muon identification in LHCb is extracted from the data using muons and hadrons produced in the $J/\psi \to \mu^+\mu^-$, $\Lambda^0 \to p\pi$ and $D^{\star+} \to \pi^+ D^0(K^-\pi^+)$ decays. The muon identification procedure is based on the pattern of the hits in the muon chambers. A momentum dependent binary requirement is used to reduce the probability of hadrons to be misidentified as muons to the 1% level, keeping the muon efficiency in the range 95-98%. Then a likelihood is built for the muon and non-muon hypotheses. Adding a requirement on this likelihood that provides a total muon efficiency at the level of 93%, the hadron misidentification probabilities are below 0.6%.

(To be submitted to JINST)

[†]Authors are listed on the following pages.

The LHCb MuonID Group

X. Cid Vidal[1,⊣], M. Gandelman[2], J.A. Hernando Morata[1], G. Lanfranchi[4], J.H. Lopes[2], D. Milanes [3], M. Palutan[4], E. Polycarpo[2], A. Sarti[4], B. Sciascia[4], F. Soomro[4] .

[1] *Universidade de Santiago de Compostela, Santiago de Compostela, Spain*
[2] *Instituto de Fsica - Universidade Federal do Rio de Janeiro - UFRJ, Brasil*
[3] *Sezione INFN di Bari, Bari, Italy*
[4] *INFN - Laboratori Nazionali di Frascati, Italy*
[⊣] *Now at European Organisation for Nuclear Research (CERN), Geneva, Switzerland*

Contents

1 Introduction

LHCb [1] is a dedicated heavy flavour experiment, designed to exploit the high $pp \to c\bar{c}$ and $pp \to b\bar{b}$ cross-sections at the LHC in order to perform precision measurements of CP violation and rare decays. Muons are present in the final state of many of the key decays, sensitive to new physics. Moreover, they play a crucial role in the determination of the flavor tagging of the neutral B mesons and are also present in the signatures of interesting electroweak and strong processes. The muon identification procedure must provide high muon efficiency while keeping the incorrect identification probability of light hadrons as muons (misidentification probabilities) at the lowest possible level. The pion misidentification is one of the major sources of combinatoric background for decays with muons in the final state. It is also important to keep the other hadron misidentification probabilities at low levels so that rare decays can be separated from more abundant hadronic decays with similar or identical topology.

This paper presents the performance of the muon identification in LHCb, obtained from the data taken in 2011, corresponding to approximately $1\,\text{fb}^{-1}$. In Section 2, a brief description of the LHCb spectrometer and the muon detection system is given. The muon identification algorithm is discussed in Section 3. The method used to extract the muon efficiency and the misidentification probability from data is explained in Section 4. Finally, the performance results are presented in Section 5, followed by the conclusions in Section 6.

2 The LHCb experiment and the muon system

The LHCb detector [1] is a single-arm forward spectrometer. A vertex locator (VELO) determines with high precision the positions of the vertices of pp collisions (PVs) and the decay vertices of long-lived particles. The tracking system includes a silicon strip detector located in front of a dipole magnet with an integrated field of around 4 Tm, and a combination of silicon strip detectors and straw drift chambers placed behind the magnet, allowing the momentum determination of charged particles with a resolution of σ_p/p $\sim$0.4(0.6)% at a momentum scale of 3(100) GeV/c. Charged hadron identification is achieved with two ring-imaging Cherenkov (RICH) detectors. The calorimeter system consists of a scintillator pad detector, a preshower, an electromagnetic calorimeter and a hadronic calorimeter. It identifies high transverse energy hadron, electron and photon candidates and provides information for the trigger.

The muon system [2] is composed of five stations (M1-M5) of rectangular shape, placed along the beam axis. As shown in Fig. 1, stations M2 to M5 are placed downstream the calorimeters and are interleaved with iron absorbers 80 cm thick to select penetrating muons. Station M1 is located in front of the calorimeters and is used to improve the transverse momentum measurement in the first level hardware trigger. The total absorber thickness in front of station M2, including the calorimeters, is approximately 6.6 interaction lengths. The major part of the system is equipped with multiwire proportional chambers (MWPC) with Ar/CO2/CF4(40:55:5) as gas mixture. Only

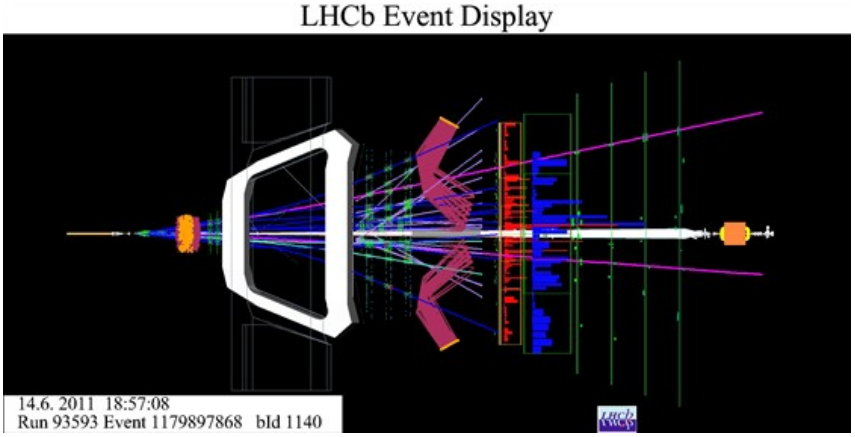

Figure 1: Schematic view of the LHCb experiment, displaying one event recorded in 2011, where 2 muons are identified (purple tracks). This is one of the best $B_s^0 \to \mu^+\mu^-$ candidates selected from the 2011 data [3]. The muon stations are seen as the five green vertical lines, the second one placed just after the calorimeters, shown as the rectangles with red and blue bars representing the energy deposition along the direction transverse to the beam.

the inner part of the first station is instrumented with triple-GEM detectors filled with Ar/CO2/CF4(45:15:40).

The chambers are positioned to provide with their sensitive area a hermetic geometric acceptance to high momentum particles coming from the interaction point. In addition, the chambers of different stations form projective towers pointing to the interaction point. The detectors provide digital space point measurements of the particle trajectories, supplying information to the trigger processor and to the data acquisition (DAQ). The information is obtained by partitioning the detector into rectangular logical pads whose dimensions define the x, y resolution in the plane perpendicular to the beam axis. Each station is divided into four regions, R1 to R4 with increasing distance from the beam axis. The linear dimensions of the regions R1, R2, R3, R4, and their segmentation scale in the ratio 1:2:4:8. Each muon station is designed to perform with an efficiency above 99% in a 20 ns time window with a noise rate below 1 kHz per physical channel, which was achieved during operation, as described in [2].

The muon system provides information for the selection of high transverse momentum muons at the trigger level and for the offline muon identification. This document refers to the latter procedure, which uses only the information from the 4 stations located after the calorimeters. The muon identification in the trigger system is described in [4].

3 The muon identification procedure

The muon identification strategy in the LHCb experiment can be divided in two steps:

- a loose binary selection of muon candidates based on the penetration of the muons through the calorimeters and iron filters, which provides high efficiency while reducing the rate of hadrons to the percent level;

- computation of a likelihood for the muon and non-muon hypotheses, based on the pattern of hits around the extrapolation to the different muon stations of the charged particles trajectories reconstructed with high precision in the tracking system.

3.1 IsMuon binary selection

The binary selection, hereafter denominated IsMuon (true for tracks identified as muons and false otherwise), is defined according to the number of stations where a hit is found within a field of interest (FOI) defined around the track extrapolation. The number of stations required to be fired is a function of track momentum (p), as shown in Table 1. The sizes of the fields of interest also depend on the particle momentum and are defined according to the expected multiple scattering suffered by a muon when traversing the material. The FOI are parameterized separately for the 4 regions of the 4 different stations downstream the calorimeter in both x and y directions according to:

$$\mathrm{FOI} = a + b * \exp(-cp).$$

The parameters a, b and c have been determined using muons from a full detector Monte Carlo simulation [5].

Momentum range	Muon stations
3 GeV/c $< p <$ 6 GeV/c	M2 and M3
6 GeV/c $< p <$ 10 GeV/c	M2 and M3 and (M4 or M5)
$p >$ 10 GeV/c	M2 and M3 and M4 and M5)

Table 1: Muon stations required to trigger the IsMuon decision as a function of momentum range.

For tracks passing the IsMuon requirement, the muon identification can be further improved by a selection based on the logarithm of the ratio between the likelihoods for the muon and non-muon hypotheses (muDLL).

3.2 Muon and non-muon likelihoods

The likelihoods are computed as the cumulative probability distributions of the average squared distance significance D^2 of the hits in the muon chambers with respect to the linear extrapolation of the tracks from the tracking system. True muons tend to have a much narrower D^2 distribution, close to zero, than the other particles that are incorrectly selected by the IsMuon requirement.

The average squared distance significance is defined as:

$$D^2 = \frac{1}{N}\sum_i \left\{ \left(\frac{x^i_{closest} - x^i_{track}}{pad^i_x} \right)^2 + \left(\frac{y^i_{closest} - y^i_{track}}{pad^i_y} \right)^2 \right\} \quad (1)$$

where the index i runs over the fired stations, $(x^i_{closest,i}, y^i_{closest})$ are the coordinates of the closest hit to the track extrapolation point for each station $(x^i_{track}, y^i_{closest})$ and $pad^i_{x,y}$ correspond to one half of the pad sizes in the x,y directions.

The D^2 distribution for muons depends on the multiple scattering and, therefore, on the momentum (p) and polar angle (θ) distributions of the analyzed sample. In order to avoid a dependence of the muon likelihood on the calibration sample (with particular p and θ), the tuning of the muon likelihood is performed separately in momentum bins and muon detector regions (which correspond to 4 intervals of θ).

The non-muon likelihood is calibrated with the D^2 distribution for protons, since the other charged hadrons (pions or kaons) selected by IsMuon will present a D^2 distribution with a component identical to the protons and a component very similar to the true muons, due to decays in flight before the calorimeter. For protons, the hits in the muon system found around the track extrapolation are essentially due to three sources: hits from punch-though [6] protons, hits from true muons pointing to the same direction of the proton or random hits. The last two are at first order uncorrelated to the proton momentum while the first one can present some momentum dependence, less important however than the dependence expected for muons. Hence, the tuning of the non-muon likelihood is merely performed separately for the 4 muon system regions, due to their different granularity.

The likelihood for the muon (or non-muon) hypothesis is then defined, for each candidate, as the integral of the calibrated muon (or proton) D^2 probability density function from 0 to the measured value, D^2_0.

The results presented in this document are obtained with a muon likelihood calibrated with muons from $J/\psi \to \mu^+\mu^-$ decays selected from the data taken in 2010, as described in Section 4. The non-muon likelihood has been calibrated with a Monte Carlo sample of decays $\Lambda^0 \to p\pi$.

The D^2 distributions for muons, protons, pions and kaons obtained from data are shown in the left part of Fig. 2. The distributions of the logarithm of the ratio between the muon and non-muon hypotheses (muDLL) are shown in the right panel of Fig. 2. More details about the selection of the particles used to make these plots and to extract the performance are given in Section 4.

3.3 Combined likelihoods

The muon and non-muon likelihoods presented in Section 3.2 can be combined with the likelihoods provided by the RICH systems and the calorimeters to improve the muon identification performance.

The Cherenkov angles measured in the two RICH detectors are combined with the track momentum using an overall event log-likelihood algorithm. For each track in the event, a likelihood is assigned to each of the different mass hypotheses (electron, muon, pion, kaon and proton). The RICH likelihood can differentiate between muon and other particles in particular at low momentum, below 5 GeV/c [7].

The energy deposition in the calorimeters also allows the evaluation of likelihoods for the muon (minimum ionizing particle), electron and hadron hypotheses [8].

A combined log-likelihood is then obtained for each track and for each of the different mass hypotheses by summing the logarithms of the likelihoods obtained using the muon system, the RICH and the calorimeters. In this computation, the non-muon likelihood obtained in the muon system is assigned to the electron, pion, kaon and proton hypotheses. The difference of the combined log-likelihoods for the muon and pion hypotheses (combined DLL) is then used to identify the muons.

3.4 Discriminating variable based on hits sharing

The number of additional tracks in the event which share hits with the muon candidate can be used to further discriminate actual muon candidates from fake ones. In order to reduce the fraction of misidentification due to nearby muons keeping a high efficiency for true muons, only additional IsMuon candidates sharing at least one hit and with a smaller D^2 value for the square distance significance are counted to build the observable called from now on *NShared*. Analyses which do want to reduce the probability of incorrectly identifying hadrons as muons due to this source usually select muons requiring NShared=0, but looser requirements are also possible, as can be seen from the NShared distributions of muons, protons, pions and kaons shown in Fig. 3.

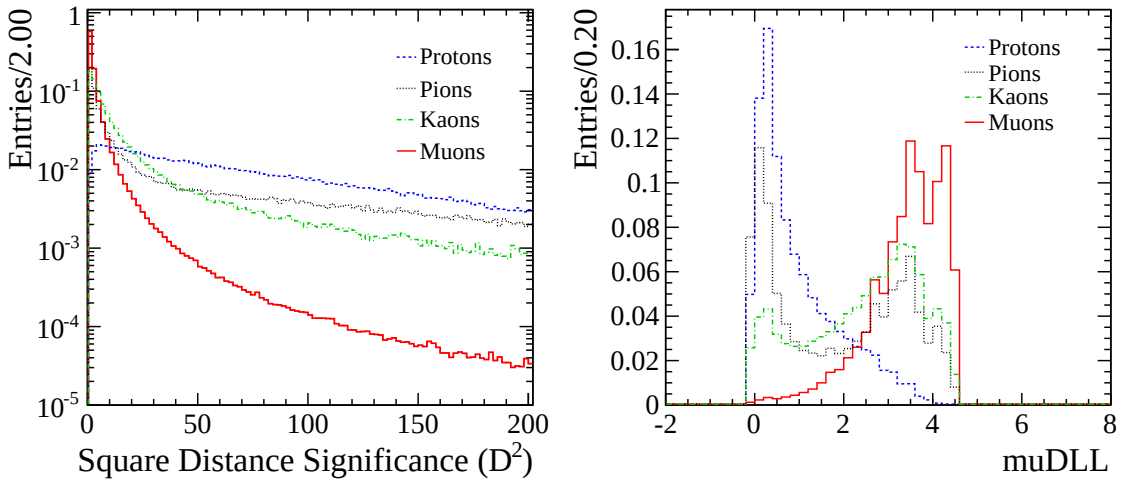

Figure 2: Average square distance distributions for muons, protons, pions and kaons (left) and the corresponding muDLL distributions (right).

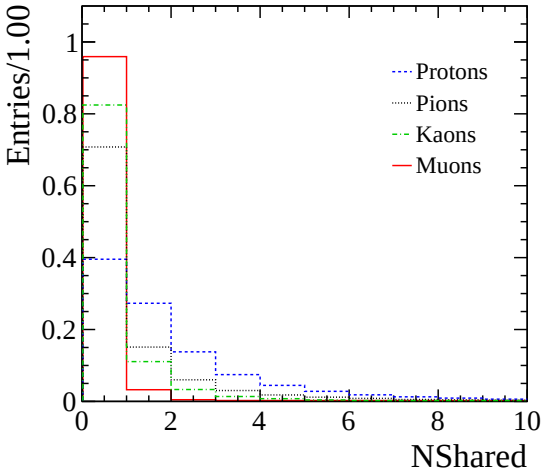

Figure 3: Normalized NShared distributions for muons, protons, kaons and pions.

4 Method for the extraction of efficiencies

In order to extract the performance of the muon identification from data, muon, proton, pion, and kaon candidates are selected with high purity from two body decays using kinematical requirements only. When necessary, the purity is improved by using a *tag and probe technique* where particle identification requirements are applied to one of the tracks (tag) while the other (probe) is used for the computation of the muon efficiency or of the hadron misidentification probability.

4.1 Selection of control samples

An abundant source of muons is provided in our experiment by the $J/\psi \to \mu^+\mu^-$ decay. By requiring the muons to have a high impact parameter with respect to the primary vertex and the reconstructed J/ψ to have a large flight distance significance and good decay vertex quality, most of the combinatorial background originating from the tracks coming from the primary vertex is removed and the sample gets enriched by $B \to J/\psi X$ candidates. In order to reduce further the combinatorial background, one of the muons is required to be identified as a muon. This is defined as the *tag* muon, while the one being probed is only required to have $p_{\rm T} > 0.8$ GeV/c.

Protons are selected from the $\Lambda^0 \to p\pi$ decays reconstructed using decay vertex quality criteria and detachment of the decay vertex from the primary one. Besides, the invariant mass obtained by assigning the π mass to the two daughters is required to be out of a window of 20 MeV/c^2 around the nominal K^0_s mass.

The $D^{*+} \to \pi^+ D^0$ ($\to K^- \pi^+$) decays are our source of pions and kaons. Once again relatively high impact parameter is required for the daughters while the D^0 flight direction is required to point to the primary vertex. To evaluate the pion misidentification probability, the tag kaon is selected using a suitable cut on the π-K log-likelihoods difference, based on the RICH information. To evaluate the kaon misidentification probability, we use as well the RICH particle identification to identify the pion. Quality criteria are used for the D^{*+} and D^0 decay vertices. A window of 25 MeV/c^2 around the nominal D^0 mass is used to exclude the doubly Cabibbo suppressed mode and the K^+K^- and $\pi^+\pi^-$ decay channels.

To avoid our results to be biased by the trigger requirements, in the J/ψ and Λ^0 samples only events triggered independently on the probe track are used; this condition has to be satisfied at both hardware and software level, as explained in [9]. For the $D^0 \to K^-\pi^+$ sample, a substantial fraction of the events would be lost by such requirement. We therefore require that the hardware trigger fires independently on the probe track (kaon or pion) and with a software trigger decision based on impact parameter and detachment from the primary vertex only, with no particle identification requirement.

After the background subtraction of selected two-body decays, the number of muon, proton, pion and kaon candidates in the 2011 data samples are 2.4, 16.1, 11.7 and 12.3 millions, respectively.

4.2 Efficiency evaluation

As a baseline method to evaluate the efficiency ϵ_{muonID} of a generic muon identification requirement denoted in this section by $muonID$ (e.g. IsMuon true or DLL greater than a given cut), we use :

$$\epsilon_{muonID} = \frac{S_{true}}{S_{true} + S_{false}}, \tag{2}$$

where S_{true} and S_{false} are the numbers of signal events satisfying and not satisfying $muonID$, extracted from data using

$$S_{true,false} = N_{true,false} - B_{true,false}. \tag{3}$$

$N_{true,false}$ are obtained by counting the number of J/ψ candidates with invariant mass lying within a signal mass window around the J/ψ mass; the number of background events within the same mass window, $B_{true,false}$, is computed by extrapolating to the signal window the mass fit done in the J/ψ sidebands.

For the proton misidentification probability, the same method is used.

The kaon and pion misidentification probabilities are also obtained with Eq. 2, but $S_{true,false}$ and $B_{true,false}$ are extracted directly from a full fit of the signal and background shapes to the invariant mass distribution of the D^0 candidates.

5 Results

The muon identification performance is presented in terms of the muon efficiency and hadron misidentification probabilities for the different requirements. In all cases, the performance is evaluated for tracks extrapolated within the geometrical acceptance of the muon detector.

5.1 IsMuon performance

The efficiency of the IsMuon requirement, ε_{IM} , is the efficiency of finding hits within the fields of interest in the muon chambers for tracks extrapolated to the muon system. In Fig. 4, ε_{IM} is shown as a function of the muon momentum, for different transverse momentum ranges. A weak dependency with transverse momentum is observed and in particular a drop of $\sim$2% is measured for the lowest $p_{\rm T}$ interval. This efficiency drop is essentially due to tracks close to the inner edges of region R1 which in principle have their extrapolation points within M1 and M5 acceptance, but are in fact scattered outside the detector. For particles with $p_{\rm T}$ above 1.7 GeV/c, the efficiency is above 97% in the whole momentum range, from 3 GeV/c to 100 GeV/c. The average efficiency obtained for the $\mu_{\rm probe}$ in the J/ψ calibration sample is ε_{IM} =(98.13 $\pm$ 0.04)%.

The misidentification probabilities $\wp_{IM}(p \to \mu)$, $\wp_{IM}(\pi \to \mu)$ and $\wp_{IM}(K \to \mu)$ are also shown in Fig. 4. The observed decrease of $\wp_{IM}$ with increasing transverse momentum is expected, since tracks with higher transverse momentum traverse the detector at higher

polar angles, in the lower occupancy regions. The proton misidentification probability is $\lesssim$0.5% for all p_T ranges and momentum above 30 GeV/c. It drops quickly with momentum for the lowest $p_{\rm T}$ ranges, reaching a plateau at about 30-40 GeV/c. The pion and kaon misidentification probabilities have a similar behavior, increasing with decreasing p_T. Above 40 GeV/c, the pion misidentification probability is almost at the level of the proton misidentification probability. At low momentum, decays in flight are the dominant source of incorrect identification, as can be seen from the difference between the pion/kaon and proton curves. While the proton misidentification probability, within the $p_{\rm T}$ intervals chosen, lies within 0.1-1.3%, the pion and kaon misidentification probabilities are within 0.2-5.6% and 0.6-4.5%, respectively. For momentum above 30 GeV/c, $\wp_{IM}(\pi \to \mu)$ and

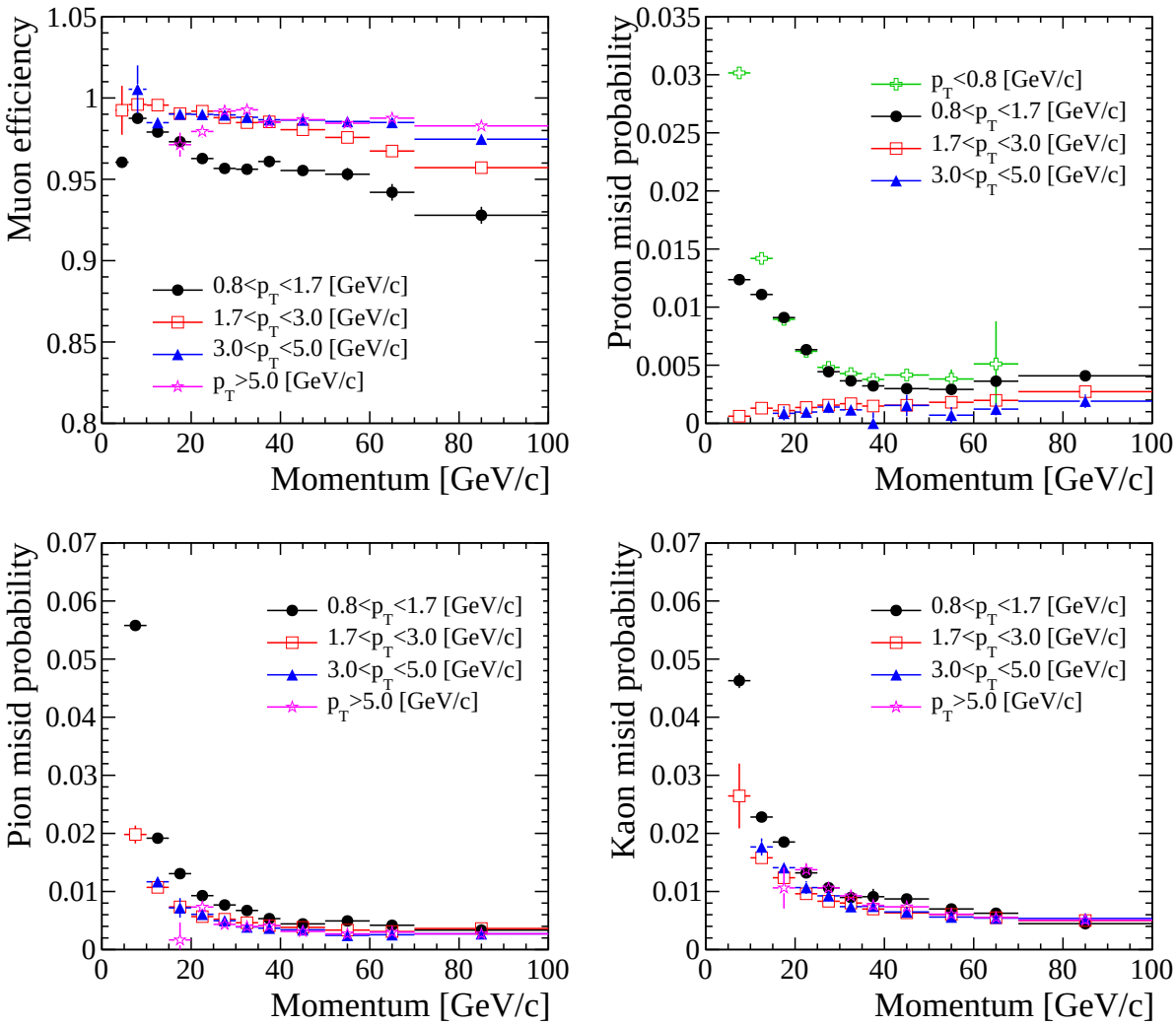

Figure 4: IsMuon efficiency and misidentification probabilities, as a function of momentum, in ranges of transverse momentum: ε_{IM} on the top left, $\wp_{IM}(p \to \mu)$ on the top right, $\wp_{IM}(\pi \to \mu)$ on the bottom left and $\wp_{IM}(K \to \mu)$ on the bottom right.

Table 2: Average IsMuon efficiency and misid probabilities in different transverse momentum intervals (%).

p_T interval (GeV/c)	muon	proton	pion	kaon
$p_T < 0.8$		1.393± 0.005	6.2± 0.1	4.3±0.1
$0.8 < p_T < 1.7$	96.94± 0.07	0.737± 0.003	2.19± 0.01	1.93±0.1
$1.7 < p_T < 3.0$	98.53± 0.05	0.149± 0.004	0.61± 0.01	0.93±0.01
$3.0 < p_T < 5.0$	98.51± 0.06	0.12± 0.02	0.40± 0.01	0.72±0.01
$5.0 < p_T$	98.51± 0.07		0.33± 0.02	0.69±0.01

$\wp_{IM}(K \to \mu)$ are practically independent of $p_{\rm T}$. At the lowest p_T range, the kaon misidentification probability is lower than the pion for the lowest momentum interval, in spite of the larger decay width of kaons to muons. Since the muon is produced with a larger opening angle with respect to the original track trajectory in kaon decays than in pion decays and in average low momentum particles decay more upstream of the detector, then the hits in the muons chambers have a higher probability to lie outside the fields of interest.

When integrated over the whole p and $p_{\rm T}$ spectra of our calibration samples, the average values for the misidentification probabilities are $\wp_{IM}(p \to \mu)$ =(1.033 ± 0.003)%, $\wp_{IM}(\pi \to \mu)$ =(1.025±0.003)% and $\wp_{IM}(K \to \mu)$ =(1.111±0.003)%. For pions and kaons, about 60% of the misidentification probability is due to decays in flight, for these particular samples. The average efficiency and misid probabilities, integrated over momentum, are also given in Table 2, for 5 different $p_{\rm T}$ intervals. There aren't enough candidates in the muon, pion and kaon samples for a measurement dependent on momentum in the lowest $p_{\rm T}$ bin. Similarly for the protons, in the highest $p_{\rm T}$ interval.

The LHCb detector has been designed to operate at the luminosity of $\mathcal{L} = 2 \times 10^{32}$ cm^{2}s^{-1}, at which the probability of having one interaction per beam crossing is maximal with respect to higher numbers. However, in the 2011 run the experiment operated in a much higher multiplicity environment than previously anticipated. The behavior of ε_{IM} and $\wp_{IM}$ was then evaluated as a function of the number of tracks which contain hits in the tracking subsystems, from the VELO to the tracking stations, as those shown in the event display of Fig. 1. No significant decrease of ε_{IM} is observed while, as expected, an increase of the misidentification probabilities is seen. The probability $\wp_{IM}(p \to \mu)$ increases by a factor 2.7 for particles with momentum in the range 3 to 5 GeV/c, when comparing events with track multiplicity smaller than 40 and events with track multiplicity between 150 and 250, which is the highest interval of multiplicity analised. At high momentum, the difference is much less important. For pions and kaons, the increase at low momentum is around 2 and drops very quickly, becoming insignificant already at 20 GeV/c. Since the FOI are smaller at high momentum, the misidentification probability becomes less sensitive to the multiplicity of the underlying event. The detailed behaviour as a function of momentum is shown in Fig. 5.

The efficiency ε_{IM} was also analysed separately for the opposite charge muons; no

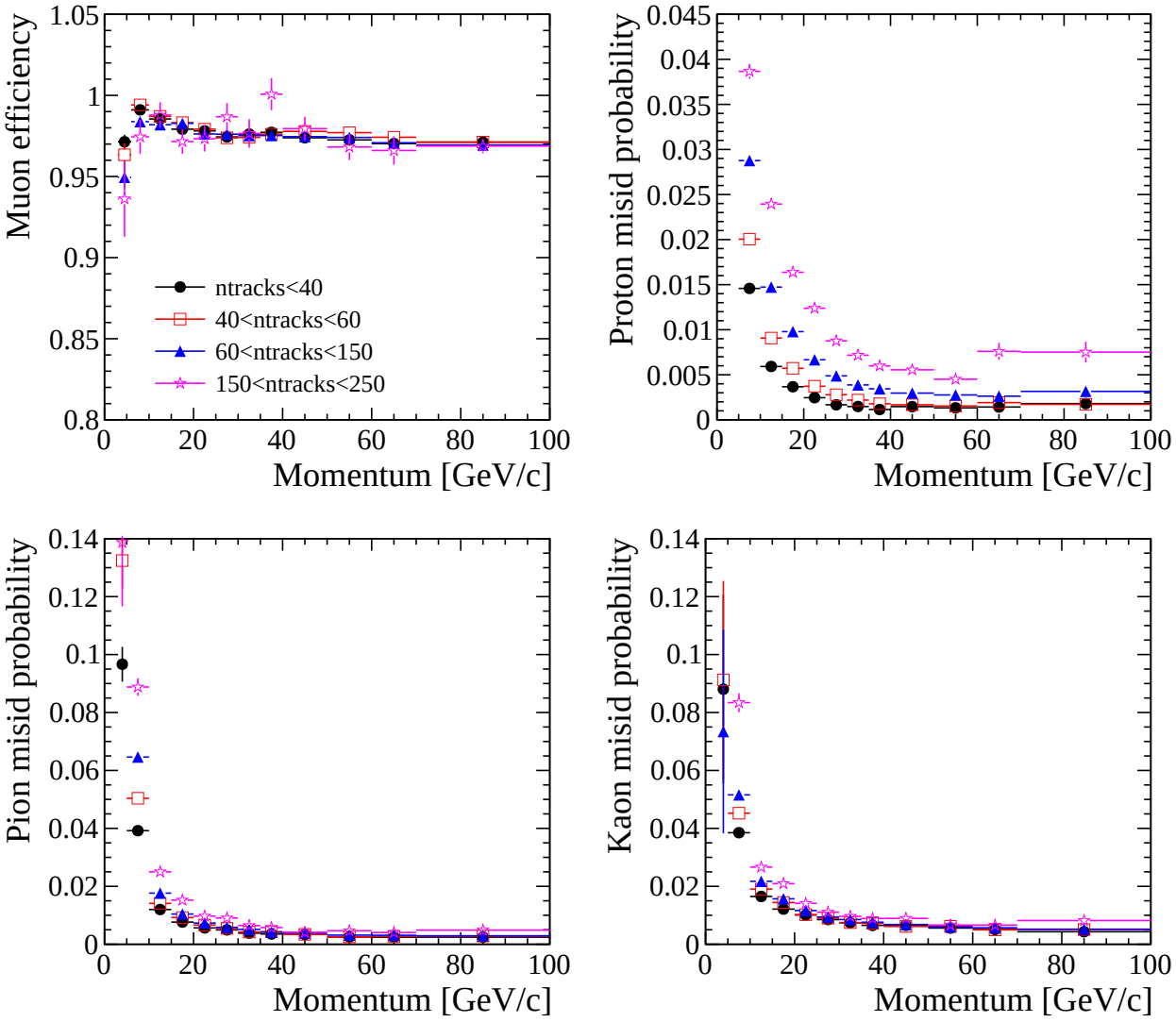

Figure 5: IsMuon efficiency ε_{IM} (top left) and $\wp_{IM}$ for protons (top right), pions (bottom left) and kaons (bottom right) as a function of momentum for different ranges of the number of trajectories reconstructed in the event (ntracks).

difference between the efficiencies is seen up to the level of the statistical fluctuations. When integrating over the whole momentum range, the relative difference is 0.09±0.08%, compatible with zero within the statistical uncertainty.

5.2 Muon likelihoods

The muon identification efficiency ($\varepsilon_{\mathrm{muDLL}}$) is measured as a function of a selection cut in the variable muDLL, for different momentum ranges, as shown in the top left part of Fig. 6. The misidentification probabilities are also shown in Fig. 6, for the same momentum

ranges. The black solid line shows the average fractions, when integrated over the whole momentum range. All the curves start at the efficiency or misidentification probability corresponding to the IsMuon requirement. The muon efficiency is independent of momentum up to muDLL$\sim$2 and for tracks with $p > 10$ GeV/c. To achieve a misidentification probability independent from the momentum, the value of the muDLL cut must depend on particle momentum. By applying a muDLL cut irrespective of the momentum, the misidentification probabilities show a strong momentum dependence.

As an example, requiring muDLL$\geq$1.74, a cut that provides a muon efficiency of 95% with respect to the IsMuon efficiency (final muon efficiency of 93.2%), we obtain as final misidentification probabilities the values 0.21%, 0.78% and 0.52% for protons, kaons and pions respectively. These average values are given for our calibration samples, which have their particular momentum and p_T spectrum and will be different for samples with different kinematic distributions.

The momentum dependence of $\varepsilon_{\mathrm{muDLL}}$ and of $\wp_{\mathrm{muDLL}}$ for particles satisfying this cut are shown in Fig. 7, compared to the IsMuon requirement alone and a tighter cut, muDLL$\geq$2.25, which reduces the muon efficiency to 90% of the IsMuon efficiency. Again, since the performance is integrated over p_T, small variations from these values are expected for different samples, in particular for the misidentification probabilities, which present a stronger dependence with transverse momentum.

5.3 Combined likelihoods

The combined DLL efficiency is shown as a function of the proton, kaon and pion misidentification probabilities in Fig. 8, together with the results obtained using the muDLL alone, allowing for a direct comparison of their performances.

The combined DLL and muDLL alone have almost the same effect on discriminating protons from muons, while the combined DLL benefits from RICH and calorimeter information, being more effective than the muon DLL alone in separating pions and kaons from muons. In particular, the average misidentification rates corresponding to a cut which provides an average efficiency of 93.2% (equivalent to the one obtained with muDLL$\geq$1.74, as previously shown) are around 0.22%, 0.65% and 0.38% for the protons, kaons and pions, respectively.

5.4 NShared performance

As mentioned in Section 3, after requiring IsMuon, an additional way of reducing the incorrect identification probability of hadrons as muons, in particular at high occupancy, is the use of a cut on NShared.

The muon efficiency is shown as a function of the pion misidentification probability for corresponding NShared cut in Fig. 9; protons are shown in the right panel of the same figure. Due to similar decay-in-flight pollution at low momentum, kaons behave as pions. The black solid line shows the average values integrated over $p > 3$ GeV/c. The blue dotted line correspond to particles in the range $3 < p < 10$ GeV/c. The red dashed lines

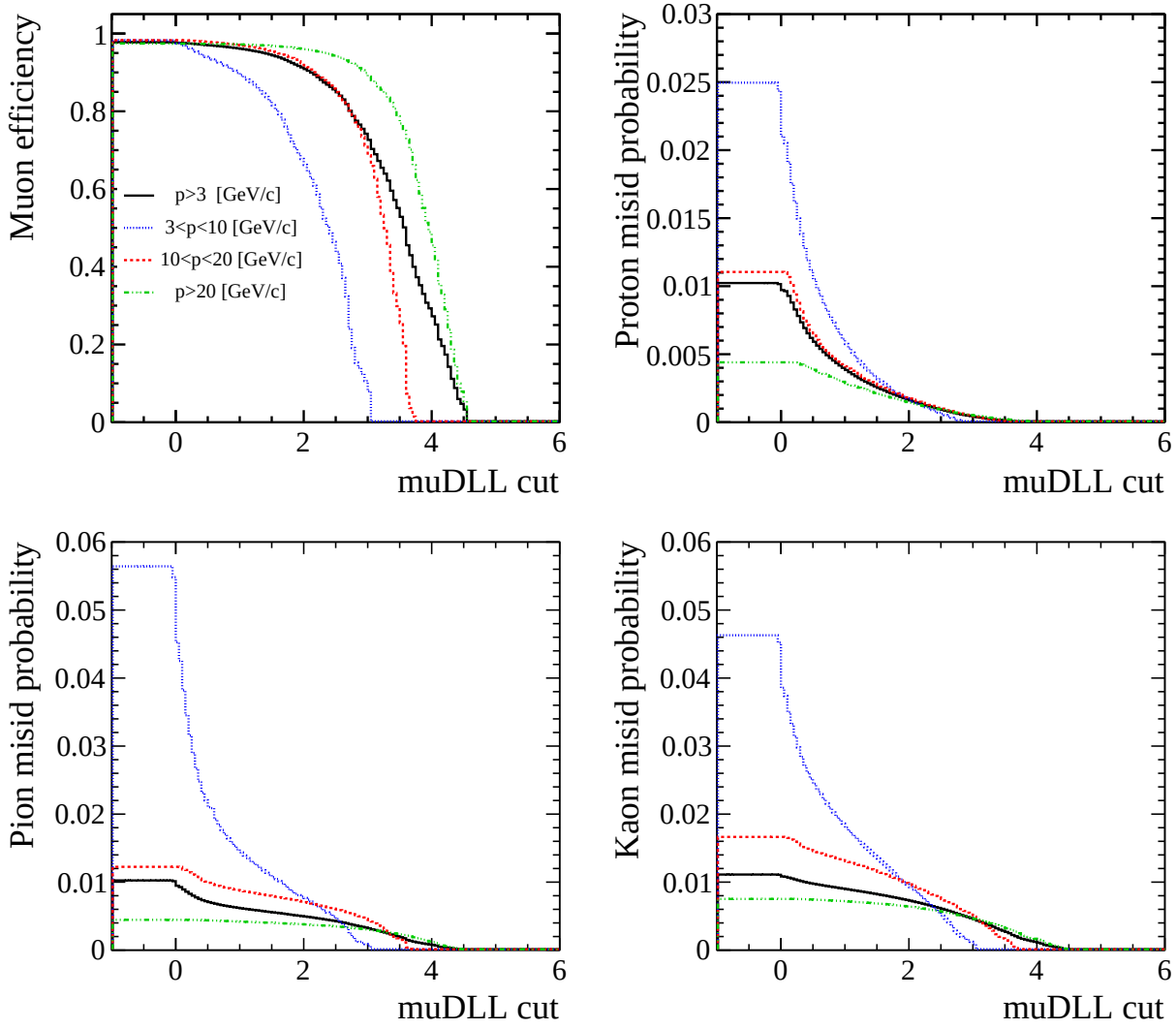

Figure 6: The efficiency $\varepsilon_{\text{muDLL}}$ as a function of muon DLL cut for muons (top left) and misidentification probabilities for protons (top right), pions (bottom left) and kaons (bottom right). The black solid line shows the average values integrated over $p > 3$ GeV/c. The blue dotted line correspond to particles in the range $3 < p < 10$ GeV/c. The red dashed lines show results for $10 < p < 20$ GeV/c and the green dashed-dotted for $p > 20$ GeV/c.

show results for $10 < p < 20$ GeV/c and the green dashed-dotted for $p > 20$ GeV/c. The NShared selection is particularly effective at low momenta, with increasing the FOI size.

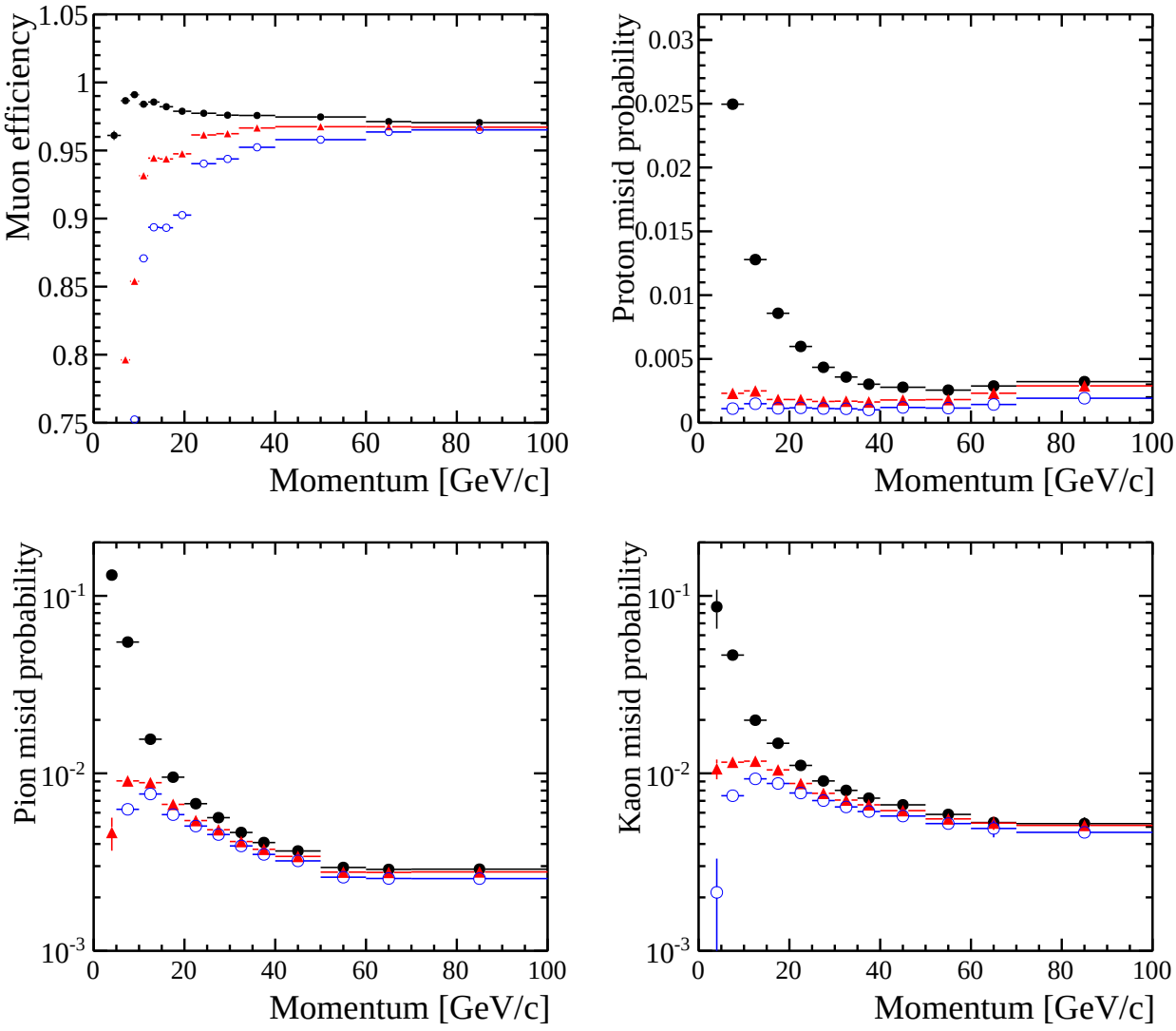

Figure 7: Muon efficiency (top left) and misidentification probabilities for protons (top right), kaons (bottom left) and pions (bottom right) as a function of the particle momentum for the IsMuon requirement alone (black solid circles) and with the additional cuts muDLL$\geq$1.74 (red triangles) and muDLL$\geq$2.25 (blue open circles).

5.5 Systematic checks

The effect of the trigger and of the method chosen to evaluate the efficiency and misidentification probabilities were investigated.

Alternatively to the requirement of the $J/\psi \to \mu^+\mu^-$ sample being triggered independently of the probe muon, a muon trigger decision based on the tag muon was used to evaluate the IsMuon efficiency. The systematic uncertainty due to the choice of trigger strategy was taken as the difference between the two determinations, which is 0.2%.

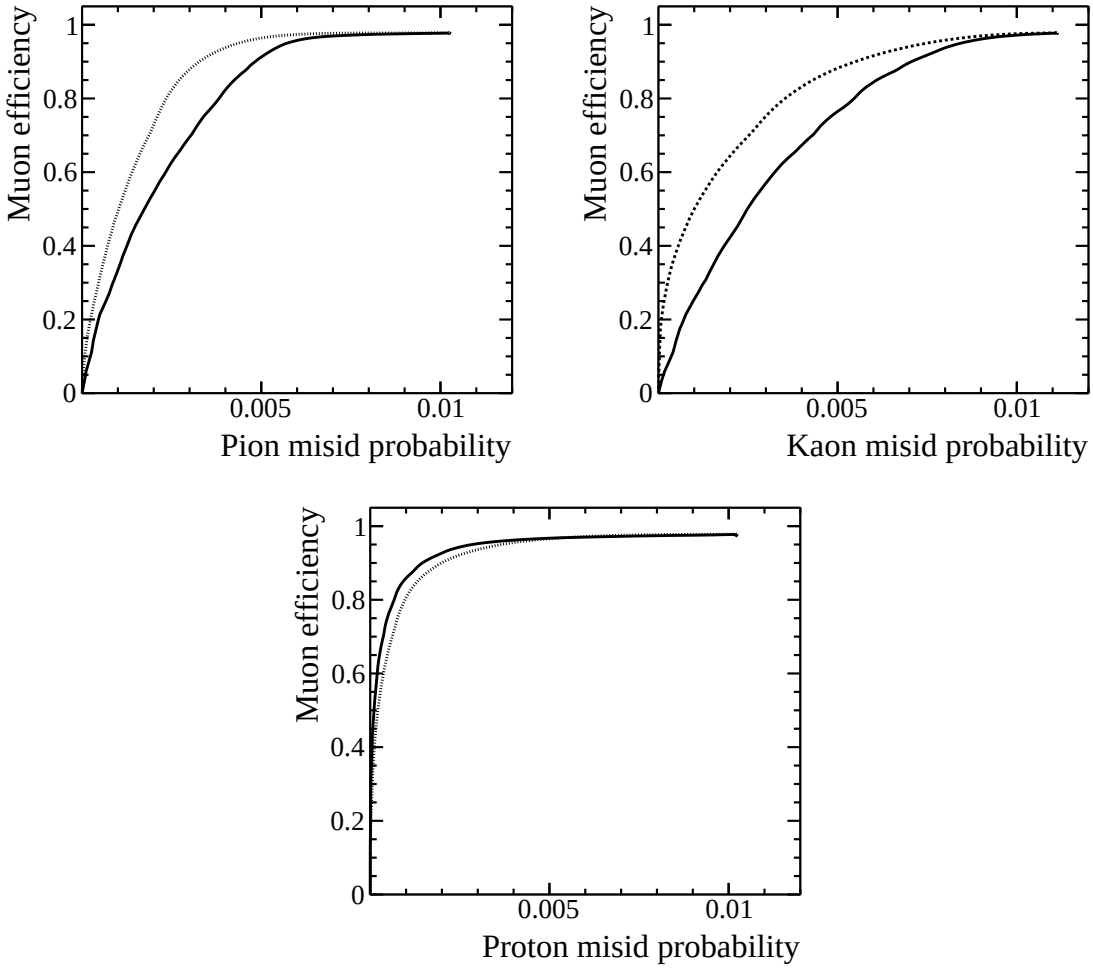

Figure 8: Average efficiency $\varepsilon_{\mathrm{DLL}}$ as a function of the pion (top left), kaon (top right) and proton misidentification probabilities for particles with momentum in the range $p > 3$ GeV/c. The dotted lines show the combined DLL performance, while the muon DLL performance is shown with a solid line.

When performing a full fit to the signal and background components of the mass distributions used to extract the yiels of signal events satisfying or not the muon identification requirements, the resulting efficiencies and proton misidentification probability rates agree within the statistical uncertainties with the results shown in Section 5.

For the pion and kaon misidentification probabilities, the effect of the trigger was studied and found to be negligible within the errors, as shown in Fig. 10 by the constant ratio between two trigger strategies. Also the systematic uncertainty related to the method used for the evaluation of the efficiency has been studied and found to be negligible apart a few bins where it is comparable with the statistical accuracy.

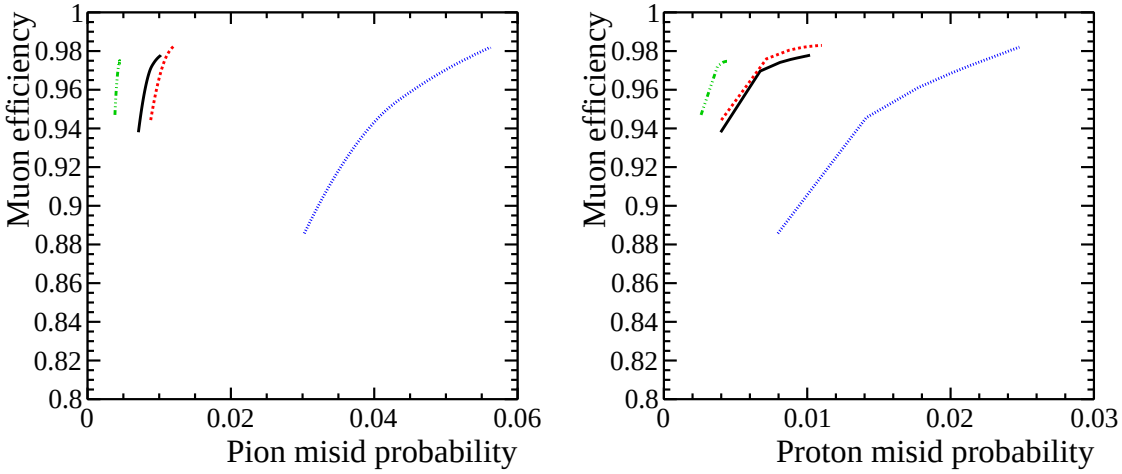

Figure 9: Efficiency $\varepsilon_{\text{NShared}}$ as a function of the pion and proton misidentification probabilities, for all particles with $p > 3$ GeV/c (black line) and for different momentum ranges separately: $3 < p < 10$ GeV/c (blue dotted), $10 < p < 20$ GeV/c (red dashed) and $p > 20$ GeV/c (green dashed-dotted).

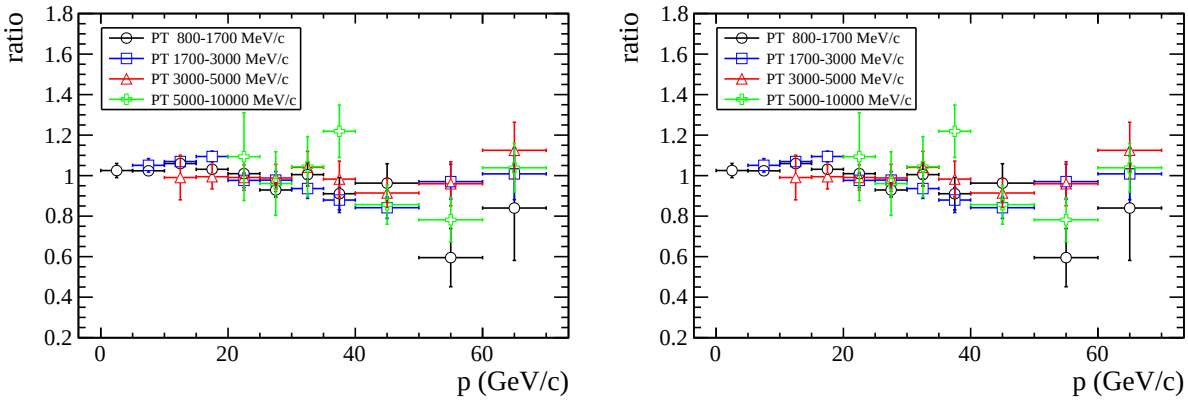

Figure 10: (a) Ratio between $\wp_{IM}(\pi \to \mu)$ obtained with the baseline trigger requirement and a trigger independent of the pion. (b) Same for the kaon. The ratios are given as a function of momentum and transverse momentum.

6 Conclusions

We have measured the performance of the offline muon identification procedure used in the LHCb experiment, using $1\,\text{fb}^{-1}$ of data taken in 2011.

The algorithm is based on a binary selection based on the matching of muon hits with the particle trajectory. For candidates satisfying this requirement, likelihoods for muon and non-muon hypotheses are built with the pattern of hits around the trajectories, which can be used to refine the selection. An additional way of rejecting fake muon candidates

is provided by a variable sensitive to hit sharing by nearby particles.

The muon identification efficiency was observed to be robust against the variation of detector occupancies and presents a weak dependence on momentum and transverse momentum. Hadron misidentification probabilities present a stronger dependence on hit or track multiplicity, however the highest increase factors are observed only for low momentum particles.

Average muon identification efficiencies at the 98% level are attainable for pion and kaon misidentification below the 1% level at high transverse momentum, using the loosest identification criterium. The performance of additional requirements based on likelihoods or on hits sharing can be tuned according to the needs of each analysis and reduce the misidentification probabilities dependence on track multiplicity.

Acknowledgements

We express our gratitude to our colleagues in the CERN accelerator departments for the excellent performance of the LHC. We thank the technical and administrative staff at CERN and at the LHCb institutes, and acknowledge support from the National Agencies: CAPES, CNPq, FAPERJ and FINEP (Brazil); CERN; NSFC (China); CNRS/IN2P3 (France); BMBF, DFG, HGF and MPG (Germany); SFI (Ireland); INFN (Italy); FOM and NWO (The Netherlands); SCSR (Poland); ANCS (Romania); MinES of Russia and Rosatom (Russia); MICINN, XuntaGal and GENCAT (Spain); SNSF and SER (Switzerland); NAS Ukraine (Ukraine); STFC (United Kingdom); NSF (USA). We also acknowledge the support received from the ERC under FP7 and the Region Auvergne.

References

[1] LHCb collaboration, A. Alves Jr. *et al.*, *The LHCb detector at the LHC*, JINST **3** (2008) S08005.

[2] A. A. J. *et al*, *Performance of the LHCb muon system*, `arXiv:1112.1346`.

[3] LHCb collaboration, R. Aaij *et al.*, *Search for the rare decays* $B_s^0 \to \mu^+\mu^-$ *and* $B^0 \to \mu^+\mu^-$, Phys. Lett. **B708** (2012) 55–67, `arXiv:1112.1600`.

[4] R. Aaij and J. Albrecht, *Muon triggers in the High Level Trigger of LHCb*, LHCb-PUB-2011-017 (2011).

[5] M. Clemencic *et al.*, *The LHCb simulation application,* Gauss*: design, evolution and experience*, J. of Phys: Conf. Ser. **331** (2011) 032023.

[6] C. Grupen, *Particle Detectors*. Cambridge university press, Cambridge, England, 1996.

[7] M. Adinolfi *et al.*, *Performance of the LHCb RICH detector at the LHC*, arXiv:1211.6759.

[8] *et al*, *Performance of the LHCb calorimeter system*, arXiv:xxxx.xxxx.

[9] R. Aaij and J. Albrecht, *Muon triggers in the High Level Trigger of LHCb*, LHCb-PUB-2011-017 (2011).